metals

MDPI

Article

Calibration of Heat Source Models in Numerical Simulations of Welding Processes

Tomasz Kik

Department of Welding Engineering, Silesian University of Technology, Konarskiego 18A, 44-100 Gliwice, Poland; tomasz.kik@polsl.pl; Tel.: +48-32-237-16481

Abstract: This article presents issues related to the methodology of the correct definition of the heat source model in the numerical analyses of welding processes. The problem of determining the input data for the stage of a heat source model definition, obtaining input data from experiments, and their proper interpretation and use in defining the numerical model was discussed. Particular attention is paid to the specificity of the problem of defining the heat source model, the way of interpreting the results of the analyses and the way of comparing them with the results of real experiments. The basic problems related to the mapping of the complex geometry of the molten metal pool and the ways to solve them were indicated. The solutions and guidelines presented in the article allow to improve the accuracy and quality of the obtained results of numerical analyses, as well as to shorten the time of preparation of computational models by reducing the number of computational iterations related to the search for the maximum consistency of the compared values and temperature cycles.

Keywords: finite element method (FEM); welding; laser; heat source model; temperature cycles; calibration; validation

check for updates

Citation: Kik, T. Calibration of Heat Source Models in Numerical Simulations of Welding Processes. *Metals* **2024**, *14*, 1213. https://doi.org/10.3390/met14111213

Academic Editor: Yu Zhang

Received: 13 September 2024
Revised: 18 October 2024
Accepted: 20 October 2024
Published: 24 October 2024

1. Introduction

Numerical analyses in modern design are an indispensable element of everyday life. However, the accuracy of numerical analyses results depends largely on the quantity but also the quality of the available input data [1,2]. The use of significant simplifications in the case of the simulation of welding processes (e.g., the shape of the simulated molten metal pool), as well as the misinterpretation of the influence of input data on the result, cause that the calculated distributions of phases, stresses, and deformations distribution in welded joints may be burdened with significant errors resulting from inaccuracies in the shape of the calculated dimensions and the shape of the molten metal pool, maximum values of temperature, and cooling rate at specific points of the model. Regardless of the type of analysis and its complexity, the welding process is characterised by many variable input data, which to a greater or lesser extent affect the geometry of the molten metal pool and, as a result, the temperature distributions [3,4].

This, in turn, translates directly into phase transformation and, finally, the resulting distributions of deformations and stresses in the analysed welded joints [5,6]. The input parameters of the process, i.e., welding current, arc voltage and welding speed, are mainly dependent on the selected welding method. They can be used to determine the total amount of heat introduced into the weld area, but this amount does not yet allow for a precise determination of the bead geometry and heat distribution in the weld joints [7,8].

Properly prepared inputs for welding process analyses contain the following [9]:

Welding process parameters (welding current, arc voltage, welding speed, laser beam power, thermal efficiency coefficient of the welding method, etc.);

Preheating temperature and inter-pass temperature;

Weld/structure geometry;

Number of beads;

Welding direction;

Boundary conditions regarding the method of clamping the weldments, the rigidity of the clamping tooling, and the possible clamping sequence;

Post-weld heat treatment parameters (if used);

Material database.

However, these data must still be complemented by knowledge of the shape of the molten metal pool itself. Only knowledge of the geometry of the simulated beads allows for the correct representation of the temperature distribution in the weld and heat-affected zone (HAZ) area. The possible residual stresses and deformations, arising first as a result of the expansion of the material during heating and then shrinkage due to cooling, depend on these geometries as well as on the temperature distribution [8]. It is therefore a fundamental part of the process of defining and calibrating how heat is delivered to the model. Both the torch angle, the type and polarity of the welding current, the type of shielding gas or the welding position will play a significant role in the formation and final dimensions of the molten metal pool. However, simplifications in the model, such as omitting some of the above-mentioned ones, often significantly affect the geometry of the bead in the numerical analyses carried out [9,10].

While parameters such as preheating temperature or the method of clamping welded elements can be defined in the form of initial boundary conditions, the geometry of the molten metal pool and the calculated temperature distributions are the results of the proper definition of the heat source model and require calibration [11,12]. Measurements of temperature, deformations, hardness distributions and tests of the macrostructure of the welded joint allow us to obtain data for comparative analysis with the results of calculations [13,14]. On this basis, with the use of specialised software that considers the phase transformations occurring in the welding process, it is possible to achieve information on the following [9]:

Values and distributions of temperature fields;

The size and shape of the bead and the heat-affected zone (HAZ);

The distribution of individual phases;

Hardness distributions in the welded joint;

Grain size;

Distributions and magnitudes of deformations;

Stress distributions after welding;

Changes in yield strength values in the weld and HAZ;

Plastic deformations;

Durability of welded joints.

2. Description of the Problem

One of the most important input parameters for the numerical analyses is the heat source model. In numerical simulations of the welding process, this is usually the only load considered in the numerical model. The nature, diversity, and variability of heat sources used in welding make its correct definition different from classic numerical analyses, where forces, moments from forces, etc., are defined. In classical mechanical analysis, the force value task solves the load problem. In the case of the welding process, when the load is a physical phenomenon that heats the material in a certain way, it is not so simple.

The main problem in welding simulations is the correct and precise determination of the amount of heat input and the mapping of the weld pool geometry [3,4]. The problem of definition and calibration of the heat source model in welding analyses of welding processes is therefore related to the development of a methodology for creating such models and conducting numerical analyses themselves [14–16].

2.1. Heat in Welding Processes

According to the first law of thermodynamics, the total energy of the system is conserved, so the energy balance at a given moment in time can be written as follows [17]:

$$\dot{E}_{in} = \dot{E}_{st} + \dot{E}_{out} - \dot{E}_{g} \tag{1}$$

where $\dot{E}_{in}$—energy introduced by the heat source, $\dot{E}_{st}$—energy absorbed by the welded material (related to the efficiency of the method), $\dot{E}_{g}$—energy generated by the system, and $\dot{E}_{out}$—lost energy.

However, the amount of energy introduced to the model by the heat source, as well as the geometry of the molten metal pool, changes not only with the change in the parameters of the heat source, but also with the welding method, the type of protective gas, or the method of metal transfer in the arc. The energy generated by the heat source is absorbed by the workpiece with a specified efficiency. The amount of heat introduced into the weld joint is represented by the following relation [15,17]:

$$Q = \eta \cdot \frac{U \cdot I}{v} \tag{2}$$

where Q—heat source power, η—thermal efficiency coefficient of the method, U—arc voltage, I—welding current, and v—welding speed.

The thermal efficiency coefficient, depending on the selected welding method, amounts to the following [9,15,16]:

Manual Metal Arc Welding: 0.8–0.9;
Submerged Arc Welding: 0.95–1.0;
Metal Active Gas (MAG) Welding: 0.8–0.9;
High-efficiency MAG Welding (buried arc): 0.85;
Metal Inert Gas (MIG) Welding: 0.7–0.8;
Tungsten Inert Gas (TIG) Welding: 0.6–0.7;
Plasma Welding: 0.6.

A solution in the form of an attempt to take these parameters into account by selecting the thermal efficiency coefficient of the method is impossible because some of them affect not only the amount of heat, but also, or even mainly, the geometry of the obtained molten metal pool. The solution to this problem should therefore be sought elsewhere—in the process of defining and then calibrating the only load in the welding process, namely the heat source model.

2.2. Heat Source Models—Defining

The software designed to conduct numerical simulations of welding processes, usually has, in addition to a solver that considers the phase transformations of the material, predefined models of heat sources. Most often, these are models in the shape of a double ellipsoid, a conical, and a surface source with a Gaussian distribution, as shown in Figure 1 [9,18].

The first of these, the model of a flat source of heat source with a Gaussian distribution (Figure 1a), is described by the following relation [15,18]:

$$Q(x,y,z) = Q_0 exp\left(-\frac{x^2+y^2}{r_0^2}\right) \tag{3}$$

where Q_0—maximum heat flux density, x, y, r_o—geometric parameters describing the heat source model.

This model is very often used in modelling the surface treatment process with a laser beam, but in the past, it was also used in modelling the process of gas and manual arc welding [19–21].

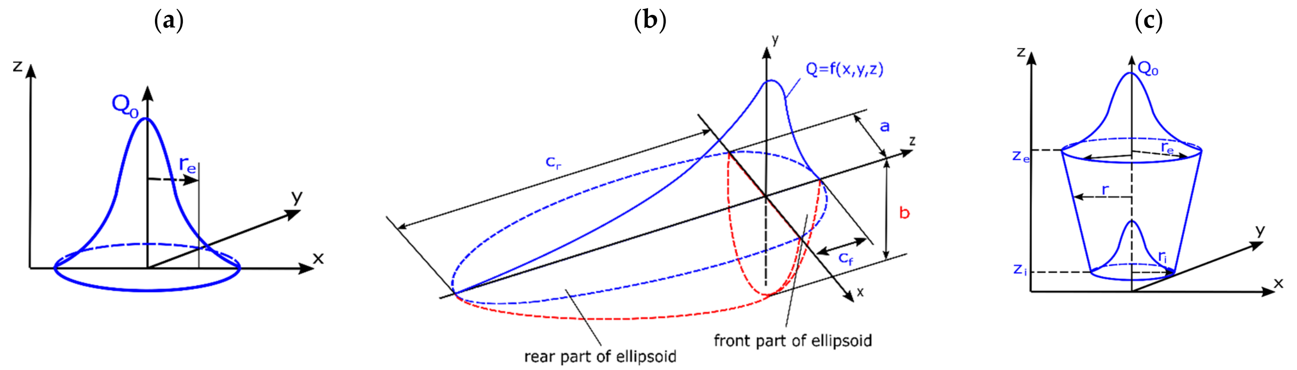

Figure 1. Scheme of standard: (**a**) model of a 2D Gaussian distribution, (**b**) double ellipsoid, and (**c**) 3D volumetric conical model heat source models used in numerical simulations of welding [18].

The mathematical description of the second of the mentioned models, the double ellipsoid-shaped model (also called the Goldak model, Figure 1b), are the two equations that describe both parts of the ellipsoids independently [16,22]:

- For the front model part:

$$Q_f(x,y,z) = \frac{6\sqrt{3}f_f Q}{abc_f\pi\sqrt{\pi}} exp\left(\frac{-kx^2}{a^2}\right) exp\left(\frac{-ly^2}{b^2}\right) exp\left(\frac{-mz^2}{{c_f}^2}\right) \quad (4)$$

- For the rear model part:

$$Q_r(x,y,z) = \frac{6\sqrt{3}f_r Q}{abc_r\pi\sqrt{\pi}} exp\left(\frac{-kx^2}{a^2}\right) exp\left(\frac{-ly^2}{b^2}\right) exp\left(\frac{-m\cdot(z - v(\tau - t))^2}{{c_r}^2}\right) \quad (5)$$

where Q_f, Q_r—volumetric heat flux density in the front and rear part of the model, Q—amount of heat introduced by the source, a, b, c_f, c_r—parameters describing the width, penetration depth and length of the model, k, l, m—model shape factors, f_f, f_r—parameters for the description of the energy distribution in the front and rear part of the model, whereby

$$f_f = \frac{2}{\left(1 + \frac{c_r}{c_f}\right)},\ f_r = \frac{2}{\left(1 + \frac{c_f}{c_r}\right)},\ f_f + f_r = 2 \quad (6)$$

x, y, ξ—coordinates describing the position of the model, where:

$$\xi = z - v(\tau - t) \quad (7)$$

τ—total bead welding time.

The double ellipsoid model is the most used heat source model in simulations of arc welding processes [22,23].

The third model, used mainly in the case of modelling welding heat sources with high energy density [8,18], is the volumetric, three-dimensional conical model (Figure 1c), which is described by the following equations [15]:

$$Q(x,y,z) = Q_0 exp\left(-\frac{x^2 + y^2}{r_0^2(z)}\right) \quad (8)$$

$$r_0(z) = r_e + \frac{r_i - r_e}{z_i - z_e}(z - z_e) \quad (9)$$

where Q_0—maximum heat flux density, r_e, r_i—upper and lower cone radius, z_e, z_i—parameters defining the height of the model, and x, y, z—coordinates that describe the position of the heat source model.

2.3. Heat Source Models—Modifications and Calibration

Correct representation of the molten metal pool geometry, and thus the determination of the parameters describing the mathematical heat source model, requires knowledge that can be obtained based on experimental tests based on measurements made on metallographic samples, as shown in Figure 2. During the calibration procedure, the parameters describing the created model must be defined in such a way that the result in the form of the calculated temperature distribution and the geometry of the molten metal pool corresponds to the geometry of the weld pool obtained in welding tests on real samples. While the surface model with the Gaussian distribution (Figure 1a) is a model usually used in simulations of surface treatment with, e.g., a laser beam, the definition of this model is relatively simple, and the volumetric models (Goldak's model and the conical model—Figure 1b,c) require more attention [14,15,24].

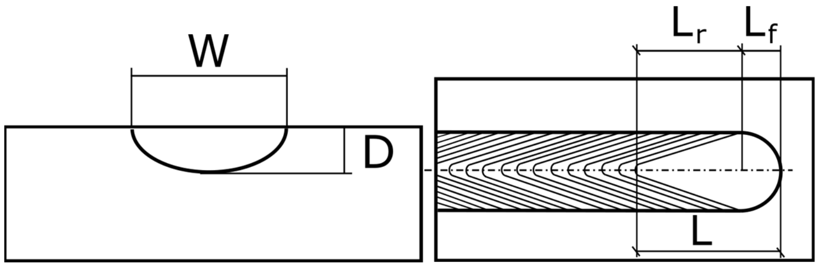

Figure 2. Scheme for measuring the size of beads geometry: W—bead width, D—bead penetration, L—molten metal pool length, L_r—length of the rear part, L_f—length of the front part of molten metal pool.

In the double ellipsoid model (Figure 1b), the equations describe the front and rear parts of the heat source model separately. Therefore, to correctly define its geometry and dimensions, four input data are needed: the width, depth (penetration), and length of the front and rear parts of the molten metal pool. In Goldak's assumptions, the length of the front part of the ellipsoid is equal to half the width of the bead, and the rear part is twice its width [25]. In later published works, a modification of this assumption can be found, equating the length of the front part with the depth of penetration and defining the length of the rear part of the heat source model as four times the length of the front part [26]. The shape coefficients in the exponents of the equations of the standard Goldak's heat source model have a value equal to 3. By changing the values of the above-mentioned coefficients, it is possible to correct the shape of the calculated molten metal pool. The need for such a modification, e.g., MAG welding, is already mentioned in the literature [8,15]. However, even these changes do not always give satisfactory results, e.g., in the case of MIG welding, where the so-called finger shape penetration is obtained with a clear increase in the depth of penetration in the middle part of the bead. One of the examples of solving this problem by using the technique of loading selected mesh elements has already been described by the author in his publications [16,23,24].

The double ellipsoid model is the most complex model in calibration, where obtaining the correct bead geometry often requires many iterations. However, even with a simpler model such as the three-dimensional, volumetric conical model, which is mainly used to simulate welding processes with high energy concentrations, such as laser beams, electron beams or plasma arcs, users often encounter a similar problem. The bead geometries obtained in welding tests, depending on the process parameters used and the achievement of full or partial penetration of the tested samples, have the following shapes: usually even, narrow or slightly widened in the upper part, Figure 3a,b. In the case of full penetration, these are usually beads with an elongated face in relation to the remaining width of the bead and little or non-existent widening in the root, as well as beads with a clearly wider area of the back with a visible narrowing of the bead's width occurring in its central part, the so-called "hourglass" (Figure 3c). A brief analysis of the shapes possible to obtain with the use of a laser beam is sufficient to conclude that it also will be not always possible to reproduce them using a standard conical model, as shown in Figure 4 [3,6,18].

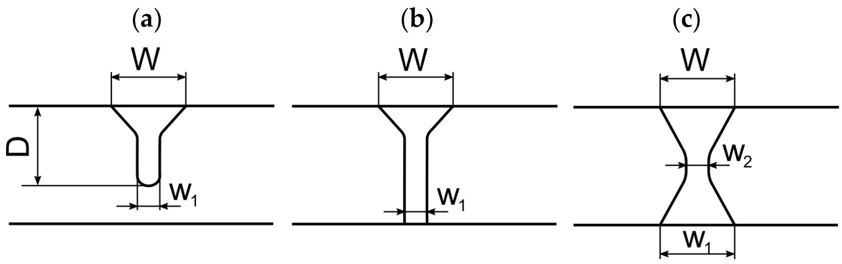

Figure 3. Example geometries obtained in the laser welding process [17].

Figure 4. View of the macrostructure of (**a**) L1 and (**b**) L2 laser disc beads on 4.0 mm thick X5CrNi18-10 steel samples (cross-section in the middle of the weld length).

The situation is similar in hybrid welding processes, where the geometries of the beads deviate from what is possible to obtain with standard models [3,27,28]. Following this lead, only the correct reconstruction of the actual shape in the molten metal pool will allow us to obtain the actual temperature distribution and the associated phase distributions, stresses and strains calculated during the analysis [29]. This is completely different from classic FEM analyses in mechanics, where the load in the form of forces or moments does not require calibration.

3. Calibration of the Heat Source Models Examples

3.1. Experimental Trials and Numerical Analyses

To explain the issues related to the creation and calibration of the heat source model with complex bead shapes, 'bead on plate' welds were made on the 80 × 50 mm X5CrNi18-10 stainless steel with a thickness of 4.0 mm. The welding tests were carried out on a disc laser station equipped with TRUMPF TruDisk 3302 with a maximum beam power of 3300 watts and a focal diameter of 200 µm. Two selected beads were tested, one with the partial and the second with the full penetration. In addition, their geometry differed from the shape of the standard conical heat model, as shown in Figure 4, Table 1.

Numerical analyses of the laser 'bead on plate' welding process were carried out using a 3D symmetrical discrete model built of 22,321 3D elements and 20,589 nodes, as shown in Figure 5a. ESI Group's VisualWeld (SYSWELD) 2023.5 software was used for numerical analysis. In order to increase the accuracy of calculations, the model mesh was densified in the bead area and HAZ. The applied boundary condition describing the heat dissipation to the environment is defined by radiation and convective heat dissipation to the environment at a temperature of 20 °C with a coefficient of convective heat transfer $\alpha = 25\ \mathrm{W/m^2 \cdot K}$ on all outer surfaces of the model, except for the plane passing through the bead centreline, on which the symmetry condition was defined. The boundary conditions simulating the sample mounting were selected to correspond to its free position on the laser welding table, as shown in Figure 5b.

Table 1. Parameters of the 'bead on plate' welding process with a disc laser beam of 4.0 mm thick X5CrNi18-10 steel samples, Figure 4.

Sample Designation	Laser Beam Power [W]	Welding Speed [mm/s]	Heat Input [J/mm]
L1	1800	16.6	108
L2	2500		150

REMARKS: type and flow rate of shielding gas: argon 5.0–15 L/min; laser beam focal diameter: 200 µm; laser beam focus position: on the top surface of the welded specimen.

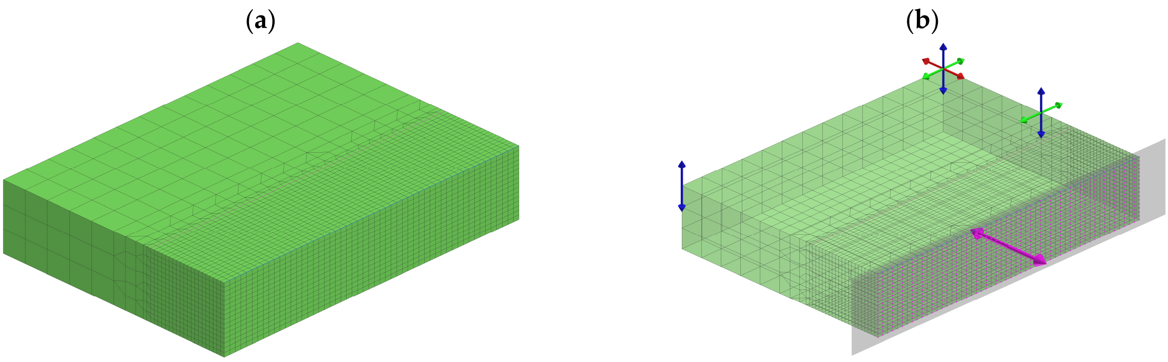

Figure 5. View of (**a**) 3D symmetric discrete model and (**b**) clamping boundary conditions of the model in the analyses of the disc laser 'bead on plate' welding process.

Numerical analyses of the disc laser 'bead on plate' welding process were carried out as a continuous analysis, using three variants of heat source models. The first of the models used was a predefined conical, volumetric model in the shape of a truncated cone (marked as CONE), as shown in Figure 1a. The geometric parameters of the conical model are defined by two radii in the upper (r_e) and lower (r_i) parts of the model and its height (z). The amount of heat introduced is determined by the heat input and method thermal efficiency coefficient, as shown in Table 2.

The second variant of the heat source model used was a popular way of constructing models, where the heat source model consisted of two or more standard [3,4,11]—in this case, volumetric conical models (marked as COMB). Each of these models moved along a determined trajectory simultaneously at the same speed, as shown in Figure 6. The selection of the division of the model into component models is made by the user. Each model is calibrated separately, but it affects the results obtained together with the other model.

The third heat source model used was a model consisting of a predefined conical volumetric heat source model, combined with the load on selected mesh elements (marked as LOAD), as shown in Figure 7. This model uses a standard conical model, which is sized to cover the shape of the mesh elements of the model, which the user defines as initially corresponding to the shape of the bead being modelled. In subsequent iterations, this area is modified to obtain a precise representation of the simulated shape.

Figure 6. Scheme of a three-dimensional, combined, volumetric conical model of a heat source: (**a**) upper part and (**b**) lower part.

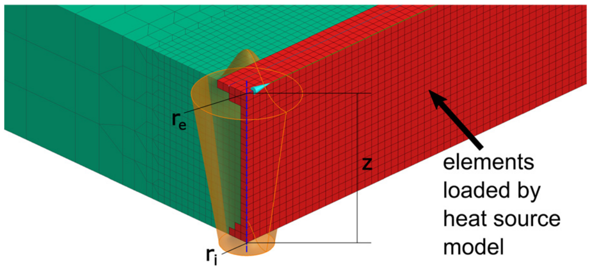

Figure 7. Heat source model scheme with definable heat input elements area.

Table 2 presents the geometric dimensions and other parameters of the calibrated heat source models, which allowed for a comparative analysis of the shape and dimensions of the simulated molten metal pools. The results of the analyses carried out with the three above-mentioned variants of defining the heat source model were compared for the cases of partial and full penetration of the sample, as shown in Table 3, Figures 8 and 9.

Table 2. Parameters of the conical heat source model after calibration of the numerical disc laser beam 'bead on plate' welding model of selected X5CrNi18-10 stainless steel with a thickness of 4.0 mm, depending on the heat source model variant used.

Sample Designation *	r_e [mm]	r_i [mm]	z [mm]	E [J/mm]	η [-]
L1_CONE	0.85	0.4	3.5	108	0.70
L1_COMB	0.75 (0.25)	0.25 (0.25)	1.25 (2.2)	54 (54)	0.70 (0.70)
L1_LOAD	0.9	0.45	3.5	108	0.67
L2_CONE	1.0	0.7	4.0	150	0.69
L2_COMB	1.6 (0.35)	0.7 (0.45)	1.0 (3.0)	85 (0.65)	0.71 (0.71)
L3_LOAD	1.5	0.75	4.0	150	0.71

r_e/r_i—radius of top/bottom base of heat source model cone; z—height of the heat source model, E—process linear energy; η—thermal efficiency coefficient of the welding method. * CONE—standard, conical model; COMB—combined heat source model consisting of two conical, volumetric models; LOAD—a model of the heat source with a defined area of influence on the elements of the model mesh; for a combined model, the values for the bottom of the models are shown in brackets.

Table 3. Influence of the applied variant of the heat source model on the geometrical dimensions of the molten metal pool of selected X5CrNi18-10 stainless steel with a thickness of 4.0 mm sample designation.

Sample Designation *	W [mm]	w_1 (w_2) [mm]	D [mm]	L [mm]
L1_measurement	1.78	0.90 (-)	3.20	3.91
L1_CONE	1.80	0.76 (-)	3.07	3.50

Table 3. *Cont.*

Sample Designation *	***W* [mm]**	**w_1 (w_2) [mm]**	***D* [mm]**	***L* [mm]**
L1_COMB	1.84	1.0 (-)	3.09	3.59
L1_LOAD	1.85	0.92 (-)	3.2	3.59
L2_measurement	2.12	1.13 (0.74)	4.0	5.39
L2_CONE	2.06	1.22 (-)	4.0	4.33
L2_COMB	2.28	1.08 (0.89)	4.0	5.28
L3_LOAD	2.16	1.10 (0.8)	4.0	5.94

W/*D*/*L*—width/penetration/length of the molten metal pool; w_1—root width (in the case of a remelting of variable width on the bead cross-section, the width of the bead at the narrowest point w_2 is given in brackets, according to Figure 3). *—designation of samples as in Table 2, measurement—real sample (from experiment).

Analysing the results of the calculations, it should be stated that for both the bead with partial and full penetration, the use of the standard, non-modified heat source model did not allow for an accurate representation of the molten metal pool geometry. A significantly better representation of the geometry of the molten metal pool was visible in the case of using a combined heat source model, as well as the use of the technique of heating selected discrete elements of the mesh. The differences between these techniques were mainly in the duration and complexity of the calibration stage of the heat source model. In the case of a model built using two separate sources, the need to divide the source into component models and to distribute the total energy of the heat source caused significant complexity of this procedure and significantly extended the duration time of the calibration stage of the heat source model.

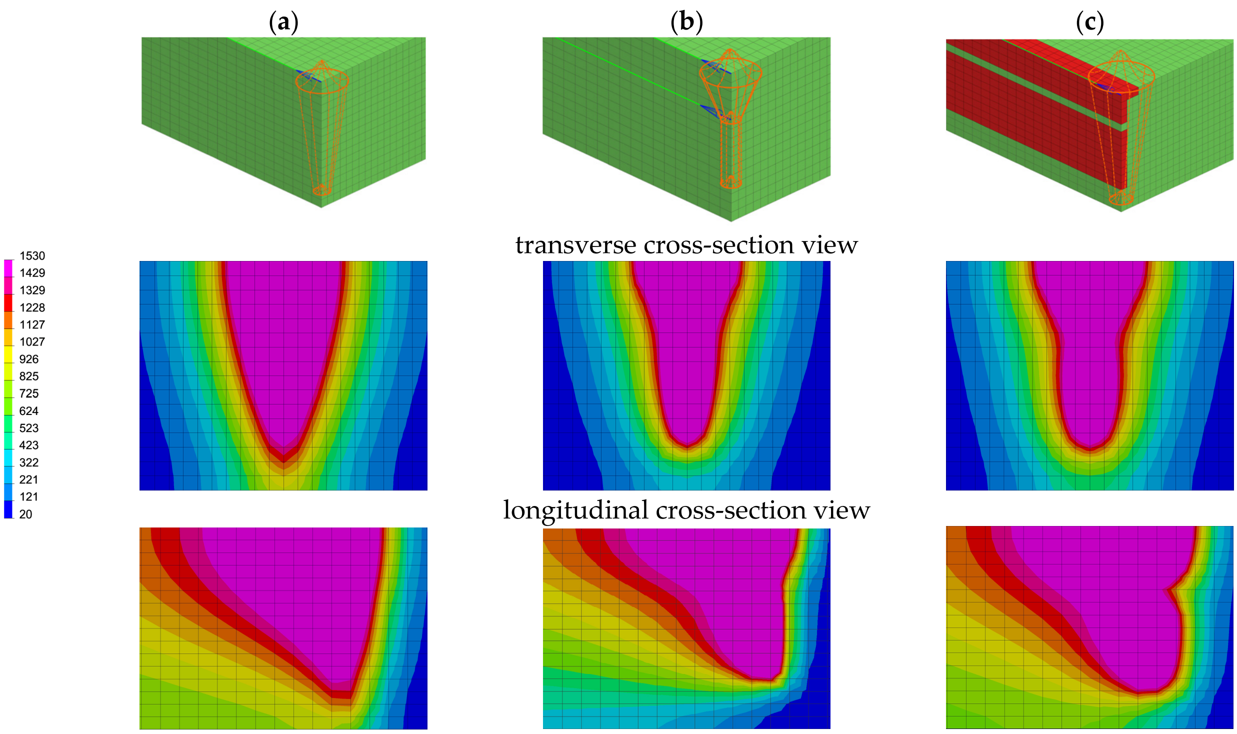

Figure 8. Comparison of the calculated temperature distributions on the cross-section of the L1 sample bead with incomplete penetration: (**a**) conical volumetric model (CONE), (**b**) combined model (COMB), and (**c**) model with defined area of mesh elements heated by heat source model (LOAD).

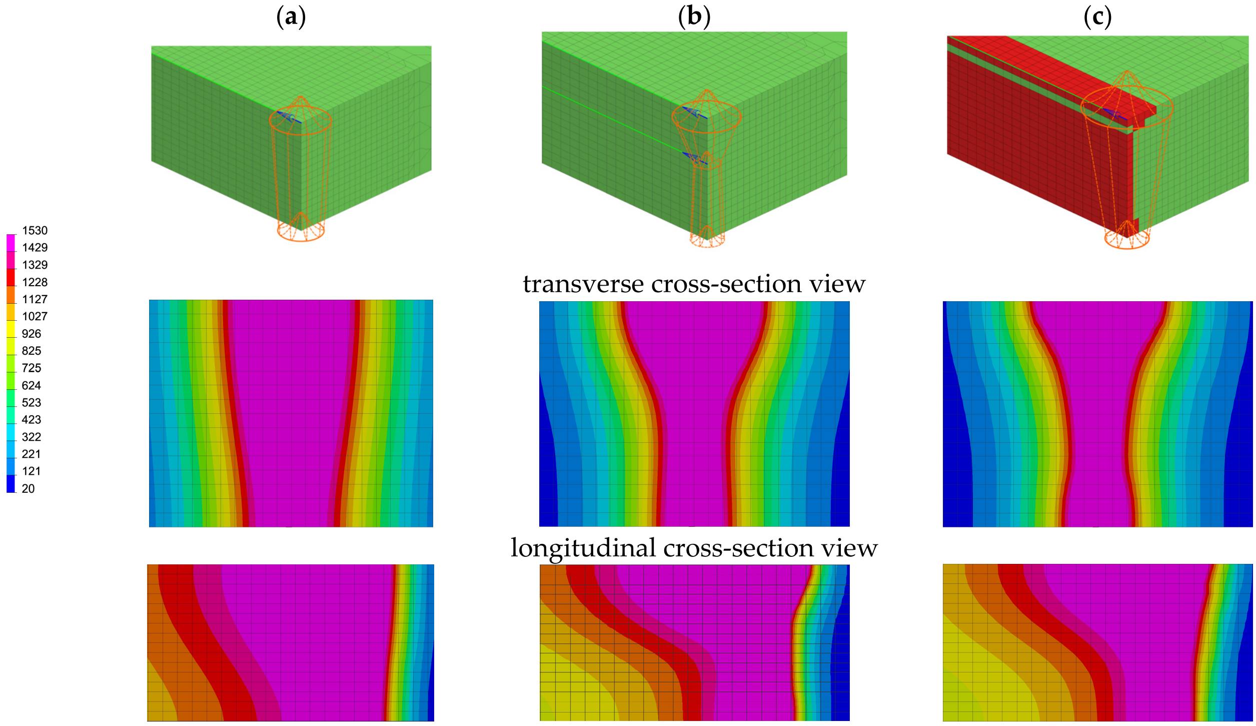

Figure 9. Comparison of the calculated temperature distributions on the cross-section of the L2 sample bead with full penetration: (**a**) conical volumetric model (CONE), (**b**) combined model (COMB), and (**c**) model with defined area of mesh elements heated by heat source model (LOAD).

In addition, it should be noted that in the case of the last variant, it is possible to reproduce the bead extension in the root area more clearly in the full penetration weld example, as shown in Figure 10. The case of using a combined model would require defining the next trajectory of motion, adding a third model at the bottom and calibrating it to determine the parameters of the heat source model.

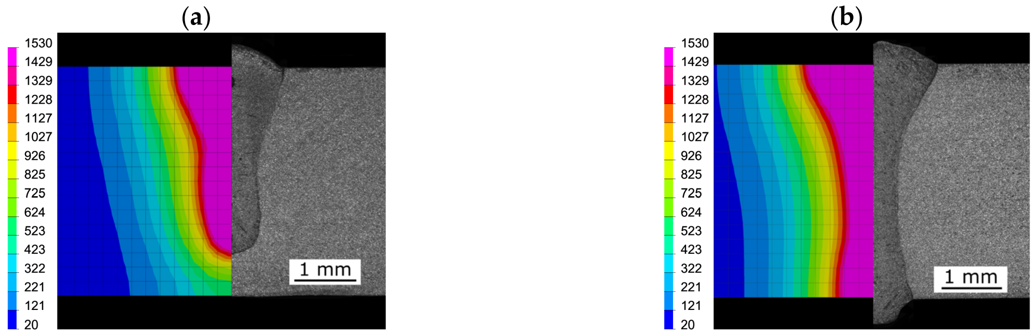

Figure 10. Comparison of the transverse cross-section shape of the molten metal pool of the numerical analysis carried out using the heat source model with the defined area of influence on the elements of the model mesh with the actual results of the 'bead on plate' welding process with a disc laser beam: (**a**) L1 sample, (**b**) L2 sample.

However, achieving a significant improvement in the quality of the molten metal pool geometry is not the only effect of the precise description of the heat source model. A comparison of the calculated thermal cycles at a selected point on the lower part of the model (located in weld centreline), in the case of the L1 sample (without full penetration) for the variant with the standard heat source model and the model with the defined area of the loaded mesh elements, showed the existence of a difference in the value of the maximum cycle temperature at about 240 °C, as shown in Figure 11a. This was mainly due to the shape of the heat source model, where the radius of the lower cone base was larger than in the model with a defined area of loaded elements to achieve the required penetration depth. However, in this case, the heat input area is determined by the selected mesh elements, not by the width of the cone model itself, as shown in Figure 7, Table 2.

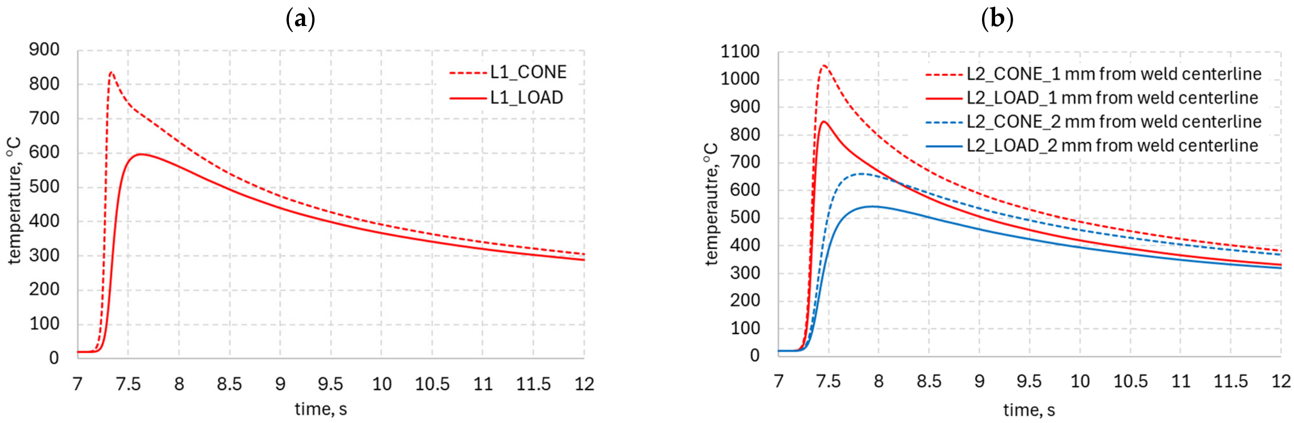

Figure 11. Comparison of the calculated thermal cycles for the variant of the application of the standard, conical heat source model and the model with the defined area of influence of the heat source model on selected elements of the model mesh in the process of (**a**) partial and (**b**) full penetration 'bead on plate' welding with a disc laser beam.

For the example of the bead with full penetration (L2 sample), the thermal cycles were determined at points located 1.0 and 2.0 mm away from the bead centreline. Differences between the standard and the modified models were visible, the difference in the maximum value of the heat cycle temperature calculated was 203 °C and 120 °C, respectively, at points 1.0 and 2.0 mm from the bead centreline, as shown in Figure 11b. The reason for this may be that analysis of the temperature distribution on the longitudinal section additionally showed that, in the standard model, the length of the root molten area is 60% longer than the others, as shown in Figure 9a. The results obtained in both cases by the combined model, consisting of two standard models, corresponded to the results obtained by using the model with the defined, loaded mesh elements, as shown in Figure 9b,c.

3.2. Measurements of Thermal Cycles of the Laser Beam Remelting Process and Interpretation of the Results in Numerical Analysis

To measure welding thermal cycles, an Agilent 34970A digital recorder from Agilent Technologies Inc. was used, with a multiplexing card with a preset sampling rate of 55 Hz. Type K thermocouples (Ni-NiCr wire with a diameter of 0.2 mm) were connected to the recorder using compensating wires and heated to the tested samples using a Labfacility L60+ capacitor discharge welder from Labfacitlity Ltd. In accordance with the PN-EN 60584-1:2014-04 standard, thermocouples were characterised by an accuracy of $\pm 0.0075 \times T$ in the temperature range from −40 to +1200 °C [30]. Thermal cycles were recorded using two thermocouples placed in the middle of the length of the tested bead on the lower surface of the welded samples, according to the scheme presented in Figure 12. In the case of the full penetration sample (L2 sample), an additional measurement was made at 2.0 mm from the bead centreline (TC1′), as shown in Figure 12.

The recorded thermal cycles of the welding process are both data for calibration and validation of the heat source model used. A comparison of the recorded and calculated heat cycles of the disc laser welding process for the case of partial penetration (L1 sample) showed that the heat cycles, calculated for the case of using a correctly calibrated, combined heat source model and a variant with a defined area of loaded mesh elements, are similar to the recorded thermal cycle, as shown in Figure 13. Using a standard, conical model, a higher maximum temperature value of the calculated thermal cycle is visible.

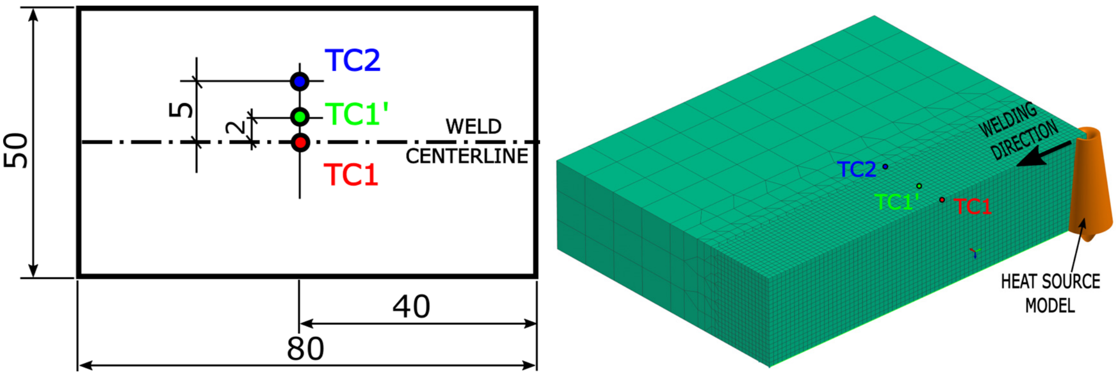

Figure 12. Scheme of the arrangement of thermocouples on the bottom of samples welded with a disc laser beam (TC1′—additional thermocouple in the case of a fully penetrated sample).

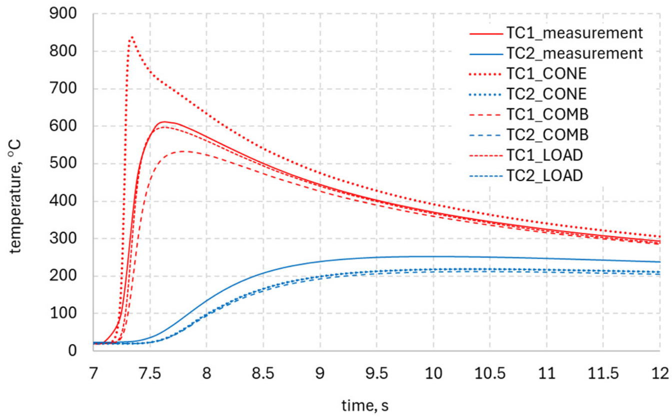

Figure 13. Comparison of the recorded and calculated thermal cycles in the disc laser beam welding process for the L1 sample and the three analysed heat source models.

However, when analysing the calculated thermal cycles in more detail, it was noticed that there are also some differences in the maximum calculated temperature of the thermal cycle at the TC1 measurement for the case of using a model with a defined area of loaded mesh elements, as shown in Figure 13. This may be due to the fact that the thermal cycle is calculated at the mesh node of the model, while, in reality, the tip of the thermocouple is not a point but has a specific dimension that covers a larger area. The result is therefore recorded as an average of the temperature value in this area. Based on the analysis of selected measurement points, it was found that the size of the tip of the thermocouples heated to the tested samples was in the range of 0.76 to 0.84 mm, as shown in Figure 14.

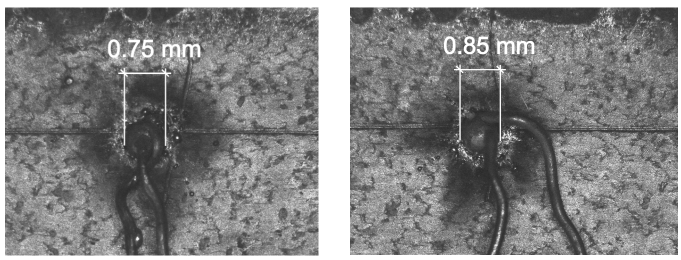

Figure 14. Examples of measuring the diameter of thermocouples used in the recording of thermal cycles of the laser welding process.

When modelling processes with high power density, the model mesh is usually highly dense in the area of influence of the heat source model to obtain a precise representation of temperature distributions. Thus, with the size of the mesh element in the model used equal to 0.25 mm, and the smallest tip of the thermocouple used in the tests (0.75 mm), as many as four mesh nodes can be accommodated, as shown in Figure 15a. The analysis of thermal cycles at these points showed that the difference in the maximum temperature in the case of nodes corresponding to the TC1 thermocouple (located in the bead centreline) reached the value of nearly 100 °C, and in the case of the TC2 thermocouple, it was about 35 °C, as shown in Figure 15b.

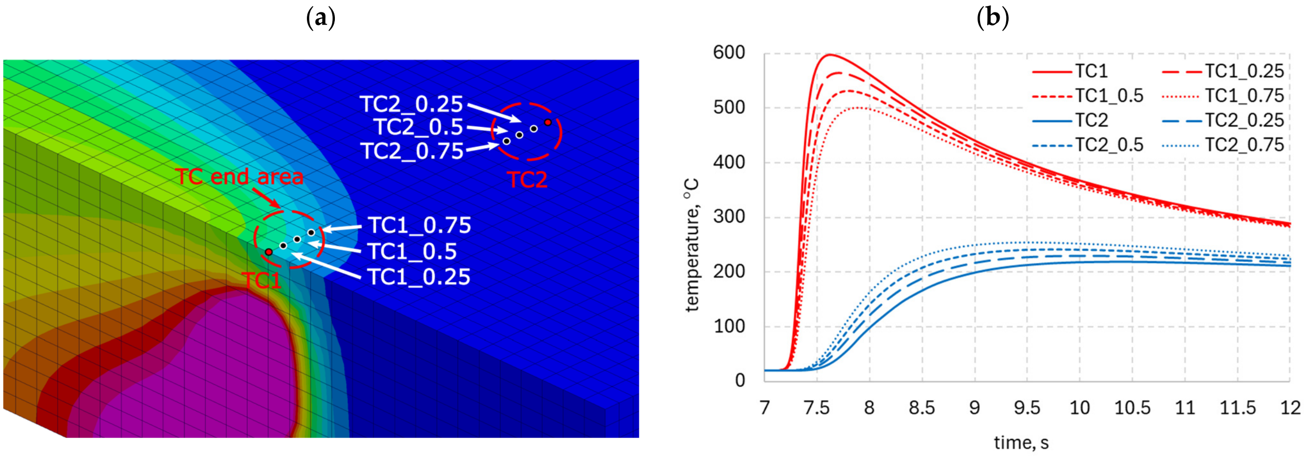

Figure 15. Illustration: (**a**) the positions of the mesh nodes used to analyses the calculated thermal cycles and (**b**) the thermal cycle courses at these points in the laser welding process.

Using thermal cycles to calibrate the heat source model, it is therefore necessary to keep this in mind and not to generate additional computational iterations, but only to compare the values in neighbouring nodes. In the analysed cases, the re-comparison of the measured cycle with the corrected calculated cycles showed a much higher agreement of the compared data for the measurement point TC1 in the case of the combined model (COMB) and the model with the defined area of the heated elements (LOAD), as shown in Figure 16a. With the use of the standard conical model (CONE) the calculated thermal cycle still reach a maximum temperature of about 100 °C higher than the measured value, as shown in Figure 16a. For the full penetration sample (L2 sample), the heat cycle measurement was made at a point offset by 2.0 mm from the bead centreline (TC1′) because the TC1 thermocouple was damaged by the heat of the liquid pool during the process, as shown in Figure 16b.

The calculated thermal cycles for the point corresponding to the thermocouples TC1′ and TC2 in the case of the model with the defined area of heated elements (LOAD) showed values similar to those recorded in the real process, both in terms of the obtained maximum temperature and the course of the analysed thermal cycles, as shown in Figure 16b.

Therefore, it should be stated that the measurements of thermal cycles in the case of the calibration stage of the heat source model are one of the basic tools allowing for precise calibration and at the same time validation of the heat source model used. However, they cannot be treated as the only experimental result that we use to calibrate heat source models due to the lack of information about the bead penetration and the shape of the obtained penetration line. However, when using thermal cycle measurements as a supplement to the macrostructure image of the bead, the development of new or modification of existing models of heat sources is possible with high accuracy with reality due to the knowledge of the process.

Infrared image recordings can also be an additional tool for obtaining information about the geometry of the molten metal pool. However, this technique has significantly more limitations than thermoelectric measurements. Metal vapours and gases, a glowing electric arc, heated instrumentation elements, as well as differences in the emissivity of the liquid and solid phase areas of the welding area cause noise as well as differences in measured values. In addition, in many cases, due to the angle of observation, it is possible to determine only one of the dimensions, e.g., the length of the molten metal pool, and the penetration depth as well as the geometry and bead penetration are impossible to determine in these tests, as shown in Figure 17a.

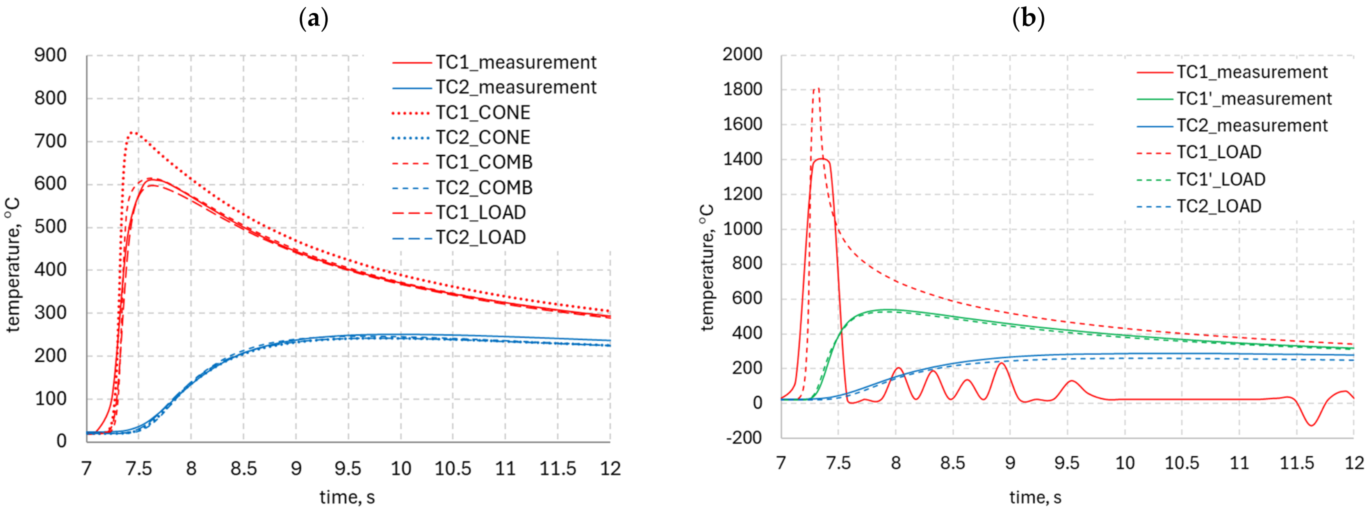

Figure 16. Comparison of the recorded and calculated thermal cycles in the process of welding with a disc laser beam: (**a**) L1 sample and (**b**) L2 sample for the three analysed heat source models structure and the corrected position of the analysed nodes of the mesh elements.

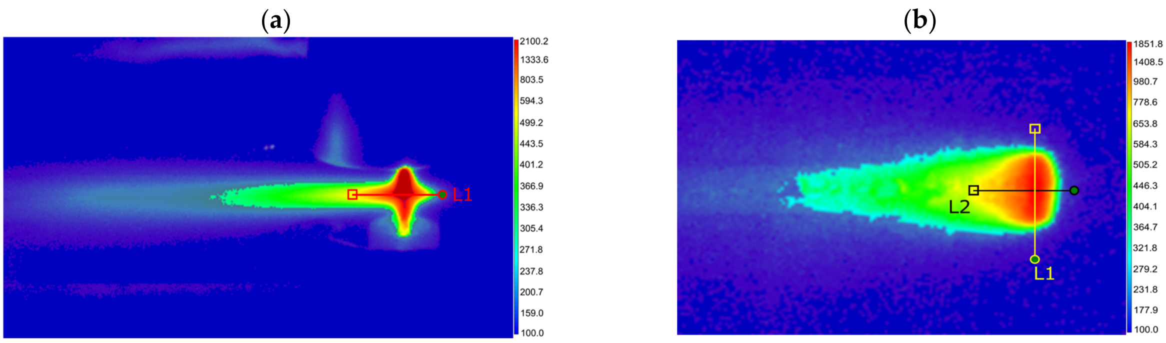

Figure 17. An example of a thermogram of the welding process: (**a**) TIG and (**b**) high-power diode laser [15].

Despite the above-mentioned significant inconveniences of this method, when properly used, it provides valuable information about the heat distribution on the analysed surface. This is particularly important when the heat distribution obtained differs from the standard one and a new heat source model is being developed. An example is the model of a heat source developed by [15,18] in the process of welding with a high-power diode laser with multimode distribution on a rectangular laser beam focus, as shown in Figure 17b. However, thermal imaging measurement cannot be the only source of data used to verify the model and rather it also has a complementary function.

A complementary function will also be performed by data from the actual welding process, i.e., distributions and values of stresses and deformations of the tested joint. Usually used at the stage of validation of the numerical model itself, they also allow us to obtain information on the correctness of the calibration of the heat source model and the mapping of temperature distributions.

4. Conclusions

The welding tests and numerical analyses carried out allowed us to conclude that the correct representation of the usually only load of the calculation model during the simulation of welding processes, which is the heat source model, is extremely important for the calculated results of temperature distributions and the related phase distributions and residual stresses and distortions in welded joints.

The use of standard heat source models does not always allow us to receive the correct dimensions and shape of the molten metal pool, and it is necessary to modify the mathematical description of the heat source model used. The choice of more complex heat source modelling techniques, e.g., using models consisting of two or more standard, predefined models, allows for improving the quality of the representation of the actual shape of the weld. However, it complicates and extends the duration of the heat source model calibration stage due to the need to divide the amount of heat introduced into component models. The solution indicated by the author in the form of a heat introduction method with a specific mesh element loaded with a standard heat source model allows for a significant acceleration of the stage of defining the heat source model being created, while maintaining a high degree of compliance with its actual geometry obtained from real experiments, due to the reduction in the number of iterations at the stage of calibration of this model.

However, to be able to correctly represent the geometry of the modelled bead, it is necessary to compare the results of calculations at the stage of calibration of the heat source model with the image of the macrostructure of this bead, obtained through real welding tests. Without an image of the macrostructure, it is not possible to use the described techniques to improve the quality and accuracy of the calculated molten metal pool, because there is no information about its geometry, and the bead width or length of the liquid metal pool is not sufficient data to define it.

Supplementing the macrostructure image with the recorded temperature cycle waveforms allows for additional confirmation of obtaining the correct heat distribution in the weld area and validation of the defined heat source model. These measurements should be carried out in at least two places, interpreting the obtained results considering the differences between the actual size of the thermocouple tip and the size of the numerical model mesh elements, which has been shown in the presented analyses. This is the simplest and at the same time the most effective way to validate the calculation model, not only in terms of the heat source model itself, but also the correctness of the selection of boundary conditions related to the method of heat dissipation and material data.

The use of infrared temperature measurement on the surface of the welded element allows for quick verification of the calculated heat distributions; however, due to too much noise and parameters affecting the accuracy of the measurement and the lack of basic information about the penetration depth and the shape of the penetration line, the recorded thermograms can be used instead as supplementary data.

In summary, the correct calibration of the heat source model should be conducted by comparing the following:

1. Primarily the calculated and measured dimensions of the molten metal pool and HAZ on real test samples;
2. Maximal temperature values on recorded and calculated welding thermal cycles in selected places of the welded joint;
3. Shape of the recorded and calculated thermal cycle (heating and cooling rates) in selected places of the welded joint.

Funding: This research received no external fundings.

Data Availability Statement: The original contributions presented in the study are included in the article, further inquiries can be directed to the corresponding author.

Conflicts of Interest: The author declares no conflicts of interest.

References

1. Perić, M.; Nižetić, S.; Tonković, Z.; Garašić, I.; Horvat, I.; Boras, I. Numerical Simulation and Experimental Investigation of Temperature and Residual Stress Distributions in a Circular Patch Welded Structure. *Energies* **2020**, *13*, 5423. [CrossRef]
2. Wu, C.S.; Wang, H.G.; Zhang, Y.M. A new heat source model for keyhole plasma arc welding in FEM analysis of the temperature profile. *Weld. J.* **2006**, *85*, 284–291.
3. Farrokhi, F.; Endelt, B.; Kristiansen, M. A numerical model for full and partial penetration hybrid laser welding of thick-section steels. *Opt. Laser Technol.* **2019**, *11*, 671–686. [CrossRef]
4. Wang, J.; Han, J.; Domblesky, J.P.; Yang, Z.; Zhao, Y.; Zhang, Q. Development of a new combined heat source model for welding based on a polynomial curve fit of the experimental fusion line. *Int. J. Adv. Manuf. Technol.* **2016**, *87*, 1985–1997. [CrossRef]
5. Chujutalli, J.H.; Lourenço, M.I.; Estefen, S.F. Experimental-based methodology for the double ellipsoidal heat source parameters in welding simulations. *Mar. Syst. Ocean. Technol.* **2020**, *15*, 110–123. [CrossRef]
6. Flint, T.; Francis, J.; Smith, M.; Balakrishnan, J. Extension of the double-ellipsoidal heat source model to narrow-groove and keyhole weld configurations. *J. Mater. Process. Technol.* **2017**, *246*, 123–135. [CrossRef]
7. Moravec, J.; Dobránsky, J.; Bradáč, J.; Nováková, I. New methods of obtaining input data of numerical computations by using heat treatment simulator. *Appl. Mech. Mater.* **2014**, *616*, 167–174. [CrossRef]
8. Bradáč, J.; Moravec, J. The impact of selected processes and technological parameters on the geometry of the weld pool when welding in shields gas atmosphere. *Acta Polytech.* **2017**, *57*, 78–88. [CrossRef]
9. *ESI Group: Welding Simulation User Guide, Sysweld Manual*; ESI Group: Bagneux, France, 2016.
10. Bjelić, M.B.; Radičević, B.S.; Kovanda, K.; Kolařík, L.; Petrović, A.V. Multi-objective calibration of the double-ellipsoid heat source model for GMAW process simulation. *Therm. Sci.* **2021**, *26*, 181. [CrossRef]
11. Chen, Y.; Han, J.; Li, Z.; Xia, L.; Yang, Z. An inverse method for searching parameters of combined welding heat source model. *Inverse Probl. Sci. Eng.* **2014**, *22*, 1009–1028. [CrossRef]
12. Rajabi, L.; Ghoreishi, M. Heat source modeling and study on the effect of thickness on residual stress distribution in electron beam welding. *J. Weld. Join.* **2017**, *35*, 49–54. [CrossRef]
13. Darmadi, D.B. Validating the accuracy of heat source model via temperature histories and temperature field in bead-on-plate welding. *Int. J. Eng.* **2011**, *11*, 9–17.
14. Bradáč, J. Calibration of heat source model in numerical simulations of fusion welding. *Mach. Technol. Mater.* **2013**, *11*, 9–12.
15. Kik, T. *Predykcja Własności Złączy Spawanych z Wykorzystaniem Zaawansowanych Modeli Źródeł Ciepła*; Wydawnictwo Politechniki Śląskiej: Gliwice, Poland, 2022; ISBN 978-83-7880-829-9.
16. Perić, M.; Nižetić, S.; Garašić, I.; Gubeljak, N.; Vuherer, T.; Tonković, Z. Numerical calculation and experimental measurement of temperatures and welding residual stresses in a thick-walled T-joint structure. *J. Therm. Anal. Calorim.* **2020**, *141*, 313–322. [CrossRef]
17. Incropera, F.; DeWitt, D. *Fundamentals of Heat and Mass Transfer*, 6th ed.; John Wiley: Hoboken, NJ, USA, 2007.
18. Kik, T. Heat Source Models in Numerical Simulations of Laser Welding. *Materials* **2020**, *13*, 2653. [CrossRef]
19. Tsai, N.S.; Eagar, T.W. *The Distribution of Heat Source in Arc Welding, Modelling of Casting and Welding Processes II*; Dantzig, J.A., Berry, J.T., Eds.; AIME: New York, NY, USA, 1984; p. 317.
20. Lu, Y.; Wang, Y.; Mendez, P.F. Width of thermal features induced by a 2-D moving heat source. *Int. J. Heat Mass Transf.* **2020**, *156*, 119793. [CrossRef]
21. Manca, O.; Morrone, B.; Naso, V. Quasi-steady-state three-dimensional temperature distribution induced by a moving circular Gaussian heat source in a finite depth solid. *Int. J. Heat Mass Transf.* **1995**, *38*, 1305–1315. [CrossRef]
22. Kwon, Y.; Weckman, D.C. Analytical thermal model of conduction mode double sided arc welding. *Sci. Technol. Weld. Join.* **2008**, *13*, 539–549. [CrossRef]
23. Kik, T.; Moravec, J.; Nováková, I. Application of Numerical Simulations on 10GN2MFA Steel Multilayer Welding. In *Dynamical Systems in Applications. DSTA 2017. Springer Proceedings in Mathematics & Statistics*; Awrejcewicz, J., Ed.; Springer: Berlin/Heidelberg, Germany, 2018; Volume 249. [CrossRef]
24. Kik, T.; Garašić, I.; Perić, M.; Landek, D.; Jurica, M.; Tonković, Z. Modifications of the heat source model in numerical analyses of the metal-cored arc welding process. *Energy* **2024**, *302*, 131811. [CrossRef]
25. Goldak, J.; Chakravarti, A.; Bibby, M. A new finite element model for welding heat sources. *Metall. Trans. B* **1984**, *15*, 299–305. [CrossRef]
26. Bibby, M.J.; Goldak, J.A.; Shing, G.Y. A model for predicting the fusion and heat-affected zone sizes of deep penetration welds. *Can. Metall. Q.* **1985**, *24*, 101–105. [CrossRef]
27. Skowrońska, B.; Szulc, J.; Bober, M.; Baranowski, M.; Chmielewski, T. Selected properties of RAMOR 500 steel welded joints by hybrid PTA-MAG. *J. Adv. Join. Process.* **2022**, *5*, 100111. [CrossRef]
28. Skowrońska, B.; Szulc, J.; Chmielewski, T.; Sałaciński, T.; Świercz, R. Properties and microstructure of hybrid PLASMA+MAG welded joints of thermomechanically treated S700MC steel. In Proceedings of the Metal 2018: 27th International Conference on Metallurgy and Materials: Conference Proceedings, Brno, Czech Republic, 23–25 May 2018; pp. 849–854.

29. Kumar, R.; Mahapatra, M.M.; Pradhan, A.K. A comparative analysis of the impact of fillet weld geometry on residual stress distribution in nickel-based superalloy. *Int. J. Interact. Des Manuf.* **2024**. [CrossRef]
30. Available online: https://ampero.com.pl/wp-content/uploads/2015/06/A03-TolerancjeCzujnikowTermoelektrycznych.pdf (accessed on 12 September 2024).